JOURNAL OF APPLIED ELECTROCHEMISTRY **29**: 153–163, 1999.

Structure investigations of SOFC anode cermets Part I: Porosity investigations

J. DIVISEK[1], R. WILKENHÖNER[2]

[1]*Institute of Energy Process Engineering, and* [2]*Institute for Metals in Energy Systems, Research Centre Jülich, 52425 Jülich, Germany*

Y. VOLFKOVICH

A.N. Frumkin Institute of Electrochemistry, Russian Academy of Sciences, Moscow, Russia

Received 13 May 1997; accepted in revised form 22 April 1998

The number of electrolyte/metal/pore three-phase boundaries in the SOFC anode cermet was determined in a cross-section photo according to the intercepted-segment method and given as the volume concentration of the electrochemically active phase boundary. The apparent geometrical exchange current density of hydrogen oxidation served as a relativizing measure of electrochemical activity. A direct correlation was found between the number of optically visible three-phase boundaries of 'electrolyte/nickel agglomerates/gas pores' in the unit volume of the electrode and the apparent electrochemical exchange current density. The electrode was also analysed porosimetrically by a standard porosimetry method (MSP) and the porosimetric curves were compared with the optical/electrochemical measurements of the same electrode. This comparison revealed that the sum of the integrated volume of nickel agglomerates and the single nickel particles in contact with the electrolyte give the total amount of the active nickel volume whose surface is directly proportional to the amount of optically visible three-phase boundaries in the unit volume.

Keywords: *cermet electrode*, *electrochemically active surface*, *porosimetry*

List of symbols

d	average diameters of the structural components (cm)
j_0	apparent exchange current density (A cm^{-2})
k	proportionality factor in Equation 5
n	average number of contacts between all particles present in the electrode
N	number of electrochemically active bonds (cm^{-3})
N_{t2}	two-dimensional number of three-phase boundaries determined (cm^{-2})
N_{t3}	three-dimensional number of three-phase boundaries determined (cm^{-3})
p_k	capillary pressure (bar)
r	general pore radius (cm)
r_m	main pore radius (cm)
r_1, r_2, r_3, r_4	radius as limit of integration
S_i	calculated integral internal surface (cm^{-1})
S_t	total electrochemically active internal surface (cm^{-1})
$\bar{S}_{t3}$	average electrochemically active three-phase zone surface (cm^2)
v	volume (cm^3)
V_t	liquid volume in the test sample
V_S	liquid volume in the standard sample

Greek symbols

ε	porosity
σ	surface tension (dyne cm^{-1})
θ	wetting angle (degrees)

1. Introduction

The classical construction of the SOFC fuel electrode is based on the dual structure of the Ni-metal /ZrO_2-electrolyte cermet [1]. The function of the YSZ ceramic support is to maintain the stability of the electronically conductive nickel–metal particles and to provide an anode thermal expansion coefficient acceptably close to those of the electrolyte. The YSZ part of the cermet structure also serves partially as the ionic conductor. The typical structure of the SOFC fuel electrode creates a porous system, which enables the fuel gas to penetrate from the gas supply channels to the electrochemical reaction zone, which is formed by the boundary between the metallic parts of the electrode and the electrolyte. The apparent geometrical exchange current density of hydrogen oxidation in SOFC cermets is very high and has a

value of several hundred mA cm^{-2} as shown by Holtappels [2]. If we consider the SOFC anode as a usual fuel cell electrode, applying porous electrode theory [3] it can be shown that the penetration depth of the electrical field is very small with an approximate value between 70 and 90 μm according to Table 1 and Fig. 4 from [4]. Thus, the main portion of the electrochemically active boundary is in the immediate neighbourhood of the bulk electrolyte. To gain more detailed information about the distribution of the proposed electrochemical reactive zone in the cermet anode, which corresponds to the effective boundary between the metallic and ceramic particles in the cermet structure, measurements of the porosity of the SOFC cermet were used. The volume amount (concentration) of the estimated three phase boundaries was correlated with the electrochemical properties of the cermet.

2. Experimental details

2.1. *Material preparation*

The SOFC cermets were prepared by the wet powder spraying technique (WPS) as described by Ruder *et al.* [5]. In this process, a fluid mixture or suspension of TOSOH YSZ (ZrO_2 + 8% Y_2O_3) and Baker nickel oxide particles was applied to a substrate by means of an air or manual brush. Some parts of the YSZ were partially calcinated. The original main particle size of YSZ was 0.22 μm, and after calcination was up to 16 μm. The main particle size of the NiO used was about 0.3 μm. The starting mixture consisted of three main components: powder, binder and a volatile carrier, where the latter also acts as the binder solvent. During or shortly after application, the carrier was removed by evaporation, while the binder precipitated mainly on the powder particles causing them to adhere to each other and to the substrate, so that a 'green coating' was obtained. Following a thermal step where the binder was removed, the coating–substrate combination was subjected to a controlled sintering step in which the interdiffusion bonding between the particles or between the particles and the substrate was enhanced. Since relatively small volume fractions of binder were employed (only 2–5%) the debinding step was very short and both the debinding and sintering cycles were performed continuously in a single furnace. Eight YSZ-foils, fabricated by tape casting with a thickness between 150 and 400 μm and a diameter of 19.5 mm, were used as substrate for all anodes.

With respect to the sintering conditions, three types of electrode were produced: (A) sintering for 3 h at 1300 °C; (B) sintering for 3 h at 1300 °C, followed by sintering at 1400 °C for 3 h; and (C) sintering for 3 h at 1400 °C.

The nickel oxide was reduced at 600 °C in hydrogen atmosphere. The resulting cermet material was composed of approximately 40 vol % Ni, 60 vol % YSZ. Considering the sintering temperature as a production criterion, three different kinds of SOFC cermet anodes prepared in this way were studied: 1300 °C, 1400 °C and 1300 + 1400 °C sintering temperature. The average thickness of the cermet structure was 100 μm.

2.2 *Electrochemical measurements on cermets*

To achieve stable and well defined conditions, the anodes were operated in the hydrogen oxidation mode at 950 °C and were loaded for 290 h (electrodes A), 120 h (electrodes B) and 170 h (electrodes C), respectively, in a gaseous atmosphere (H_2 + H_2O + Ar) at partial pressures of $p_{H_2} = 0.19 \times 10^5$ Pa, $p_{H_2O} = 0.03 \times 10^5$ Pa, $p_{Ar} = 0.78 \times 10^5$ Pa at an anodic current density of 280 mA cm^{-2}.

The exchange current density, as the criterion of the electrochemical activity for both freshly prepared (initial) and aged electrodes, was estimated. The necessary overvoltage values were measured with respect to the reference electrode laterally adjusted to the working electrode on the surface of the YSZ-electrolyte (Fig .1). The corresponding iR corrections were performed by means of a.c. impedance measurements. Because of the special geometry of the SOFC cells, deformations of the electric field caused by the edge effects occur, which influence the iR corrections. This effect was eliminated by the electrode preparation method, as shown in [2]. Due to the high exchange current density of the electrodes, problems arise, with respect to the possible range of overvoltages investigated. It was only possible to perform these measurements up to 60–80 mV overvoltage. Since the RT factor in the Butler–Volmer equation at 950 °C is very high, the usual Tafel plot analysis, neglecting the negative exponent factor, is inaccurate. For this reason, the exchange current density j_0 was calculated from the linearized form of the Butler–Volmer equation

Table 1. Structure analysis of the B-type SOFC cermet

d YSZ /μm	*d Ni* /μm	*d Pore* /μm	*Porosity* ε /%	*Solid fraction Ni* (*theory*) /vol %	*Solid fraction Ni* (*analytical value*) /vol %
1.6	1.8	1.8	41	40	45

d is the average diameter of the structural constituents.

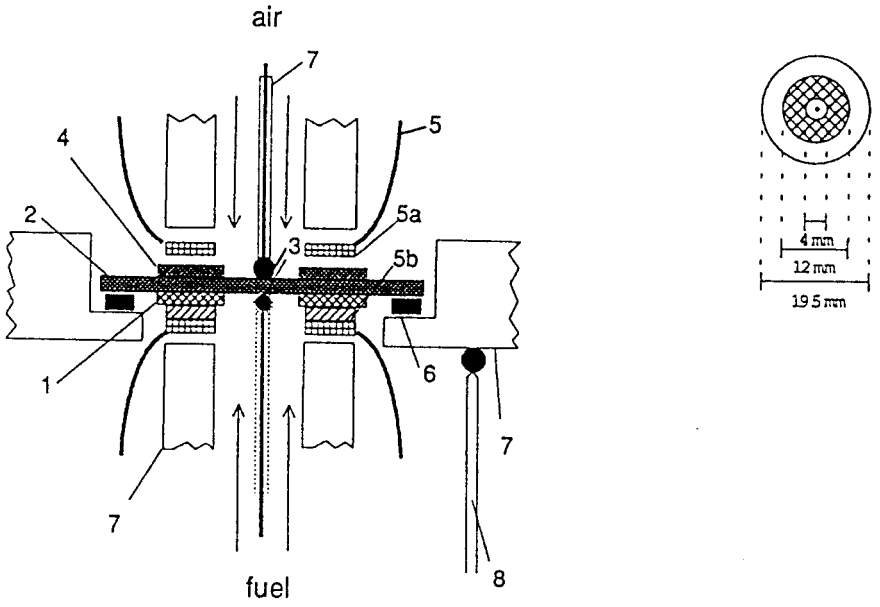

Fig. 1. Electrochemical apparatus for measuring exchange current densities. Key: (1) anode, (2) YSZ electrode, (3) Pt-reference point, (4) cathode, (5) Pt wire, (5a, 5b) Pt-, Ni-mesh, (6) gold sealing, (7) alumina and (8) thermocouple.

$$j_0 = \lim_{\eta \to 0} \frac{RT}{nF} \frac{\mathrm{d}i}{\mathrm{d}\eta} \tag{1}$$

which is valid for very low overvoltages. A typical c.d./potential curve is shown in Fig. 2. The evaluation the c.d./potential curves for higher overvoltages was only possible for two electrodes. The values of j_0 obtained in this case by means of the full Butler–Volmer equation correspond to the charge transfer coefficient $\alpha n = 0.6$, which is in good agreement with literature data [2]. It could be shown that there was no significant difference between the exchange c.d. of the freshly prepared and aged electrodes. For this reason, the j_0 values of fresh electrodes were taken as the measure of their electrochemical activity.

Since there was no difference between electrodes B and C with respect to electrochemical behaviour, only electrodes of type A and B were considered.

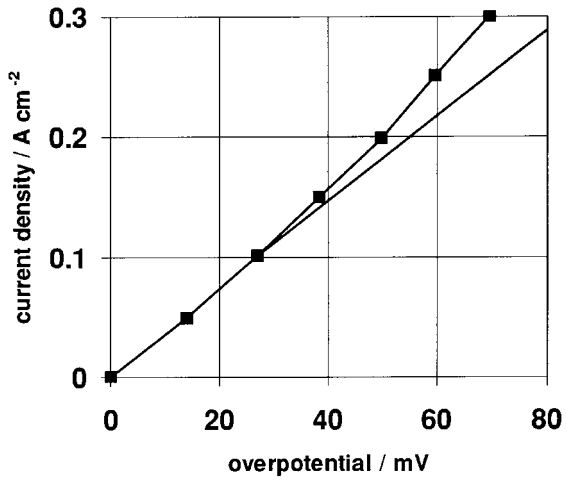

Fig. 2. Current density/overvoltage curve of the initial B electrode $t = 950\,^{\circ}\mathrm{C}$, $p_{H_2} = 0.19\times10^5$ Pa, $p_{H_2O} = 0.03\times10^5$ Pa, $p_{Ar} = 0.78\times10^5$ Pa

2.3. *Porosimetric measurements*

The porosity measurements were performed by means of a new standard porosimetry (MSP) method developed at the Frumkin Institute of Electrochemistry (Moscow) [6, 7]. MSP can be used for measurements of pore size in the range 1 to 10^5 nm. This method gives information concerning the most important properties of porous bodies analogically to mercury porosimetry. It is, however, superior to the latter with respect to the following points:

(i) MSP shows higher ranges of measured values of pore radii
(ii) MSP enables porosity measurements without destruction of sample structure
(iii) porous bodies with extremely small total pore volume are measurable

Properties (ii) and (iii) are especially useful for the determination of the porosity of the SOFC cermets.

The MSP method is based on the laws of capillary equilibrium. If two porous bodies partially filled with a wetting liquid are in contact and, consequently, are in a state of capillary equilibrium, the values of the capillary pressure p_k of the liquid in both bodies are equal. The capillary pressure can be represented by the Young–Laplace equation

$$p_k = -2\sigma \cos\theta / r_m \tag{2}$$

If for one of the two porous bodies (standard sample) the pore size distribution is known, then by measuring the equilibrium dependence of the liquid volume in the test sample (V_t) on the liquid volume in the standard sample (V_S) the pore size distribution between all porous bodies (volume of liquid V_k in the body k), the pore size distribution for test samples can be estimated. The amount of the liquid in the samples was determined by weighing. The investi-

gated electrodes were of circular shape with a diameter of 14 or 18 mm and an average thickness between 90–100 μm.

Figure 3 shows the schematic of the MSP assembly used for the determination of cermet porosity. In this Figure, the test electrode (1) is situated at the YSZ solid electrolyte (8). The counter electrode (2) on the opposite side of the electrolyte (8) was hermetically covered by a sticking plaster (3) with glue (4). In order to protect the test cell from breaking, a sufficiently soft porous interlayer material (5) was positioned between the electrode (1) and the porous standards (6,7).

2.4. *Optical cross-section evaluations*

For comparison with the porosity determination, optical evaluation of the corresponding cross-section photos of freshly prepared (initial) electrodes was carried out. For an available cross-section picture, the grain and porous structure can be evaluated by the intercept–segment method according to [8]. We defined the number of active bonds N as the number of metal–solid electrolyte grain pairs in the neighbourhood of the pores which supply each active bond with the reaction gas. To be sufficiently accurate, only micrographs containing more than 300 such contact pairs were evaluated.

3. Results

3.1. *Phase boundaries and electrochemical kinetics*

The results of the optical structure analysis of electrode B are given in Table 1. By comparing the particle sizes in the microstructure with those in the initial suspension, it can be clearly seen that the YSZ and also the Ni particles in the cermet consist of agglomerates. The micrograph is shown in Fig. 4. Metal/electrolyte boundaries in the neighbourhood of a pore which supplies the bond with electrochemically active gases were defined as electrochemically active bonds. Let the number of such bonds per cm^3 be N. The optical evaluation of the two-dimensional micrographs gave a number N_{t2}/cm^2 of three-phase boundaries. The assumption $N_{t3} = N_{t2}^{3/2} = N_{t2}^{1,5}$ is suggested as a first approximation for the transformation of the two-dimensional number N_{t2} into the three-dimensional space of the cermet anode. Since it cannot be established which of the optically determined bonds are actually electrochemically active, $N \leqslant N_{t3}$ holds with the proportionality assumption $N \approx N_{t3}$. The accuracy of the method is restricted, however, and the relative error of the estimation is approximately 30%.

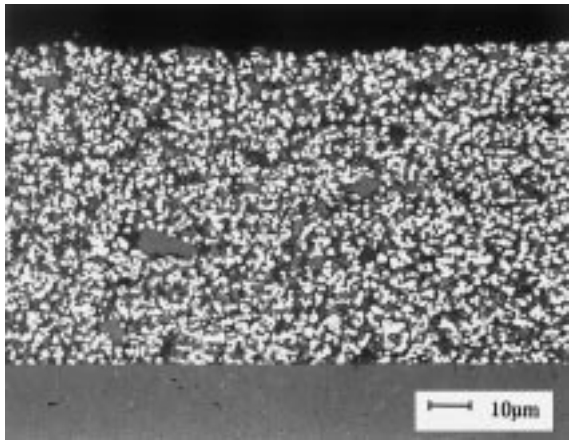

Fig. 4. Micrograph of electrode B. Bright: Ni agglomerates; grey: electrolyte; black: pores.

To determine the dependence of the electrochemical exchange current density of hydrogen oxidation on the number of active bonds, an ageing experiment was performed with a cermet anode 1 susceptible to ageing, which was fabricated for this purpose. A micrograph of the electrode in its original state was evaluated and the number of bond pairs found optically, N_{t2}, assigned to the exchange current density obtained. The electrode was then aged by operation for 16 h at 100 mA cm^{-2} in the gas atmosphere described above, the exchange current density measured and the micrograph optically reevaluated (Fig. 5). During this period the geometrically visible exchange current density j_0 changed from originally 21 to

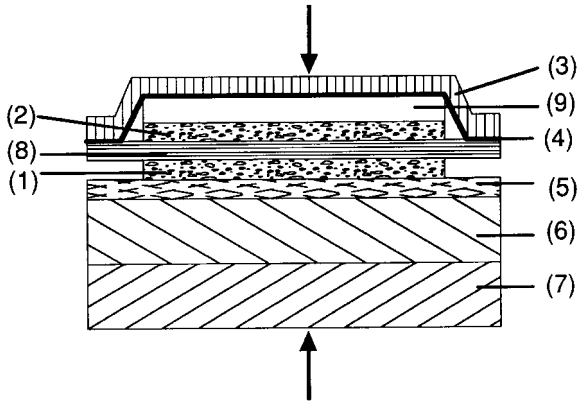

Fig. 3. Schematic sketch of the assembly for porosimetric investigations: (1) test electrode, (2) counter electrode, (3) cover, (4) protecting glue layer, (5) soft porous material, (6) porous standard, (7) porous standard and (8) solid electrolyte.

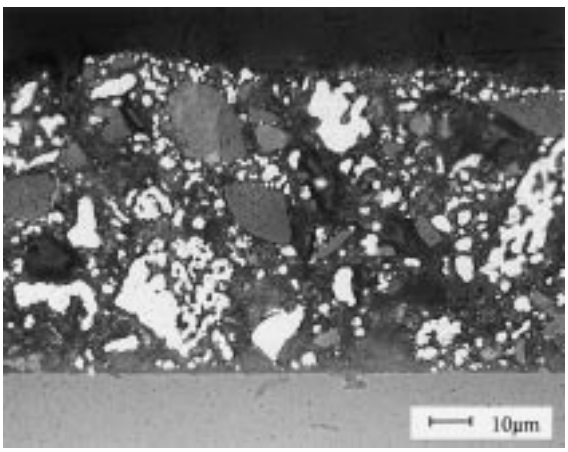

Fig. 5. Micrograph of electrode 1 after operation for 16 h. Bright: Ni agglomerates; grey: electrolyte; black: pores.

4 mA cm^{-2} and the number of bonds N_{t2} from 4×10^6 per cm^2 to 1.5×10^6 per cm^2.

After this ageing experiment, the number of three-phase boundaries N_{t2} was determined for type A and type B electrodes and electrochemical measurements were performed in the form of current density/overvoltage curves to determine the exchange current density as a criterion for electrochemical activity. All the curves obtained showed a comparable apparent electrochemical exchange current density for electrode types A and B, that is, the electrochemical properties are similar. The exchange current densities obtained, j_0, and the corresponding amounts of three-phase boundaries, N_{t2}, can be seen from Table 2. The sought dependence of the exchange current density on the three-phase boundaries N_{t3} proved to be linear through the slightly corrected recalculation $N_{t3} = N_{t2}^{1,4}$ instead of $N_{t2}^{1,5}$.

Since a linear dependence between N_{t3} and j_0 is found according to this Table, a mean surface $\bar{S}_{t3}$ (cm^2) is assigned to each three-phase zone and the following relation assumed

$$j_0 = \text{const.} \times \bar{S}_{t3} \times N_{t3} = \text{const.} \times S_t \qquad (3)$$

where S_t is the total electrochemically active internal surface of the electrode. According to [3], a linear correlation between S_t and j_0 means that the electrode has a thickness which is considerably less than the penetration depth λ of the electric field. Since the ratio $L/\lambda \approx 1$ according to Table 1 and Fig. 4 from [4], a strict linear dependency would not be expected. The observed linearity between S_t and j_0 is apparently caused by the relative error in the optical evaluation of the correlated number of the electrochemically active sites. The second possible reason for the linear dependency between S_t and j_0 may be, that the approximation $N_{t3} = N_{t2}^{1,5}$ is not strictly fulfilled in our case. With infinite layer thicknesses, a $(S_t)^{1/2}$ dependence on the current density is predicted [3, 4].

3.2. *Porosimetric structure analysis*

A total of eight type A electrodes and five type B electrodes were examined porosimetrically. The most important question to be addressed was: "Which of the structural data obtained can be used as the characteristic value and as a measure of the electrochemically active zone defined in the above sense?" A porosimetric comparison of the integral volume distribution function of four of the measured cermet electrodes is shown in Fig. 6.

If the functional dependence of the volume change, dv, on the pore radius r is known, the corresponding internal integral surface S_1 can be determined on the basis of the thermodynamically derived relation [9]:

$$S_i = 2\int_{r_1}^{r_2} \frac{1}{r}\frac{dv}{dr}\,dr \qquad (4)$$

According to [9], the value of this integral S_i , representing a measure of the envelope surrounding the pore volume v, is irrespective of the pore geometry.

The dv/dr dependence for electrodes A and B can be taken from Fig. 6. The surfaces S_i obtained by Equation 4 for electrodes A and B are shown in Fig. 7. Whereas the electrochemical exchange current densities obtained in Table 2 for A and B as well as the determined amounts, N_{t3}, of the active bonds are comparable, this is not the case for the internal electrode surfaces which vary by a factor of 3, as shown in Fig. 7.

A comparison of Table 2 and Fig. 7 therefore clearly shows that, in the case of cermet electrodes, the internal electrode surface cannot be taken as a measure of electrochemical activity. This result is not trivial since this assumption is most frequently made in the literature. The structural difference between the composition of the metallic and ceramic phases in the cermet structure was therefore investigated in two steps for two A (Aa and Ab) electrodes and one B electrode. First of all, the integral distribution of the volume v was derived for the original electrode as a function of the pore radius r. The total Ni phase was then completely extracted by dissolving it with dilute nitric acid, the electrode was washed with water and dried. This was followed by a porosimetric examination of the remaining ceramic structure. To make this optically perceptible, the micrograph of electrode Ab in the original state is shown in Fig. 8(a). In this picture, the electrolyte is bright, the nickel agglomerates are grey and the pores black (different shades from Figs 4 and 5). Figure 8(b) represents the simulated scheme of the identical area after the extraction of nickel. Figure 8(b) was obtained by tracing the white electrolyte particles from Fig. 8(a), leaving out the grey nickel particles. Figure 8(a) reflects the porosity data in Table 1. The large electrolyte agglomerates are

Table 2. Comparison of three-phase boundaries with the corresponding exchange current densities j_0 for different SOFC anode cermets

Anode	*Three-phase boundaries*		*Exchange current density j_0 /A cm^{-2}*
	N_{t2}/cm^{-2}	N_{t3}/cm^{-3}	
1 (Aged after 16 h)	1.5×10^6	4.4×10^8	0.004–0.005
1 (Initial state)	4.0×10^6	1.8×10^9	0.021–0.025
A	3.3×10^7	3.4×10^{10}	0.260–0.340
B	2.8×10^7	2.7×10^{10}	0.280–0.380

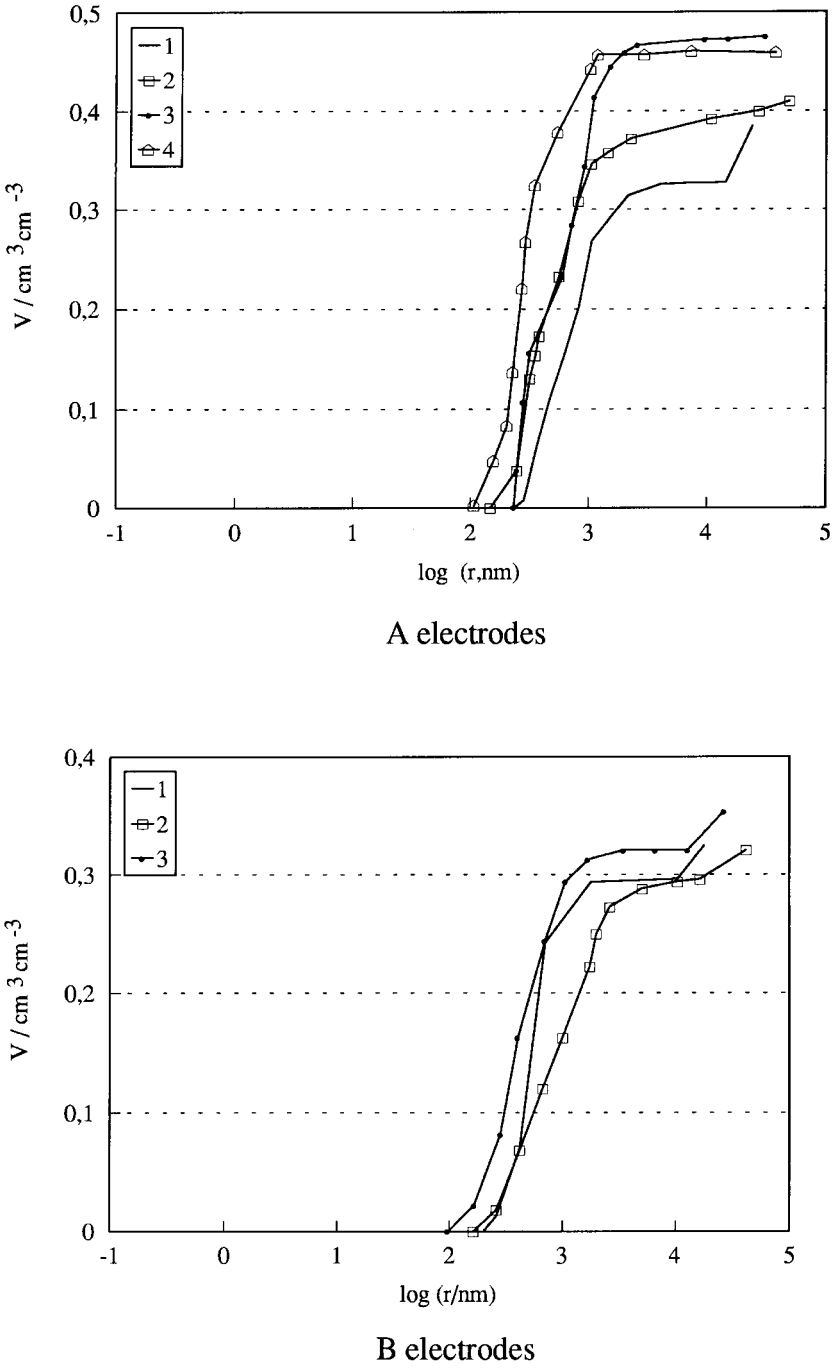

Fig. 6. Integral volume distribution as a function of pore radius.

between 10 and 20 μm in size, while the particles originating from the uncalcined powder are correspondingly smaller (1–2 μm) and comparable in size to the nickel agglomerates, the latter being, on average, somewhat larger than the electrolyte particles. This also corresponds to the data in Table 1. After dissolving the nickel out of the cermet an 'island-type' structure results as shown in Fig. 8(b), consisting exclusively of the ceramic electrolyte fractions.

The results of the porosimetric comparative analysis of the original cermet anodes with the ceramic residual structure are shown in Fig. 9. The first ascent of curve 2 occurs at pore radius r_1 (only visible for Aa). Curve 1 starts in each case at pore radius r_2 and the principal ascent of curve 2 at r_3. The minimum in difference curve 3 is reached at a pore radius r_{min}. At pore radius r_4, which is approximately 1000 nm in size, the difference curve changes into a plateau. The porosity changes are basically only visible in a pore radius region between 100 and 1000 nm. As expected, the integral curves for the ceramic residual electrolyte structure display a greater porosity than the original electrode. The smallest pores in the pore radius region between r_1 and r_3, which extends from 100 to 250 nm and is only completely characterized and discernible for electrode Aa, are only found in the ceramic electrolyte phase. For electrodes Ab and B, this first region can no longer be identified on the scale

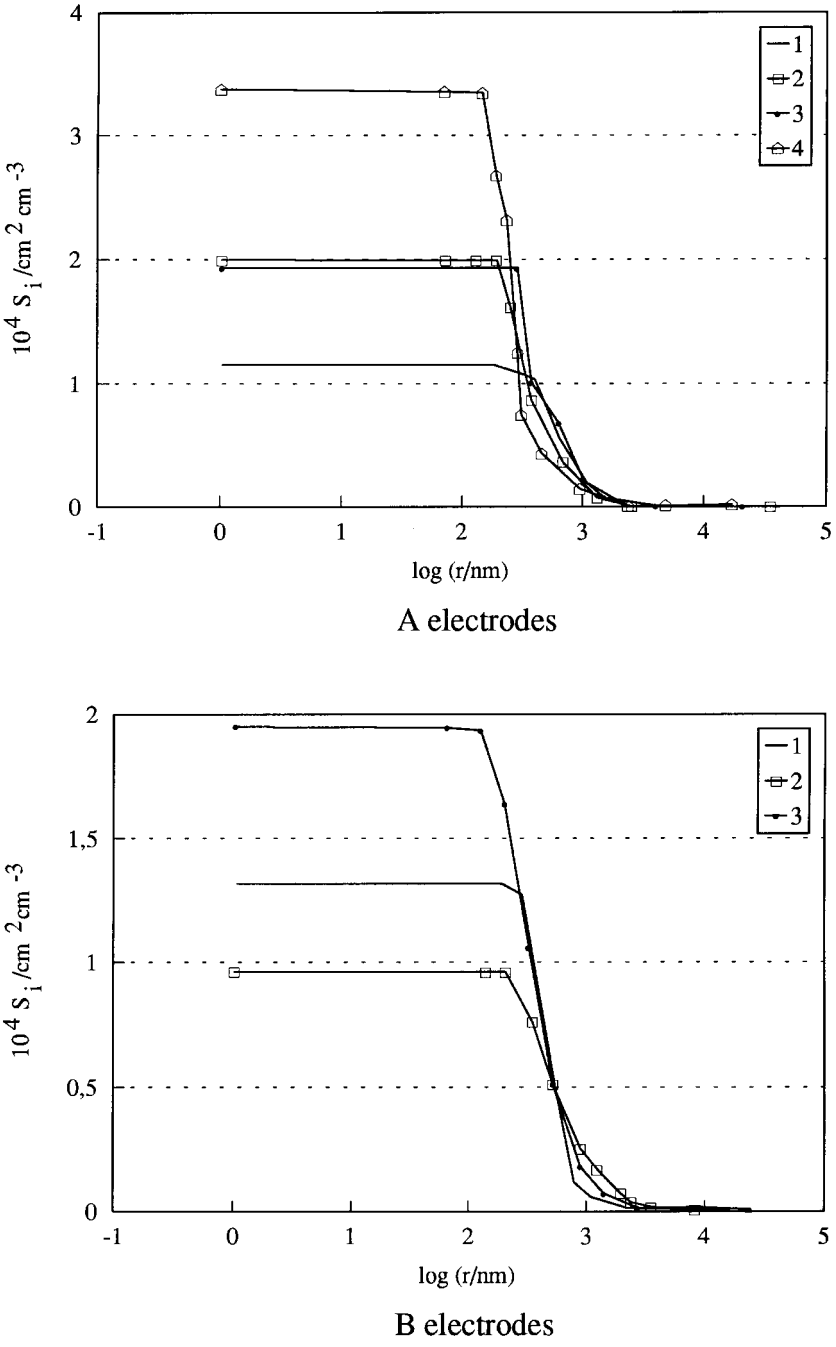

Fig. 7. Integral distribution of the internal surface as a function of pore radius.

shown. Together with micrograph 8(a), this curve analysis permits the following model concept shown schematically in Fig. 10.

The double structure of the cermet electrode consists of single nickel particles, nickel agglomerates and small sintered ceramic particles which may form a larger grain without agglomerate structure. Single grains (*1*) in the $r_1 < r_3$ region between the ceramic particles fill the volume v_1. The small Ni single grains are only present in appreciable concentrations in electrode Aa. The nickel agglomerates composed of several particles (*2*) are between $r_{min} < r_4$ in volume v_2. Their internal structure consisting of single grains also becomes visible by the difference curve in the $r_2 < r_3$ pore radius region.

After removing the nickel particles and agglomerates, a new structure results characterized by the formation of new pores (*1*a) and (*2*a) in the former regions $1(v_1)$ and $2(v_2)$. The negative values of curves 3 in Fig. 9, originating in the $r_2 < r_{min}$ porosity region, are caused by the internal porosity of the Ni agglomerate volume (*2*), which is not in contact with the electrolyte and is no longer present after the nickel has been dissolved, as well as by the interstices between the agglomerates and the electrolyte. The sum of the integrals of volume distribution curve 3 between the limits of integration $r_1 < r_3$ (volume v_1, in which it is identical with curve 2) and $r_{min} < r_4$ (volume v_2) is assigned to those nickel fractions whose envelope is at least

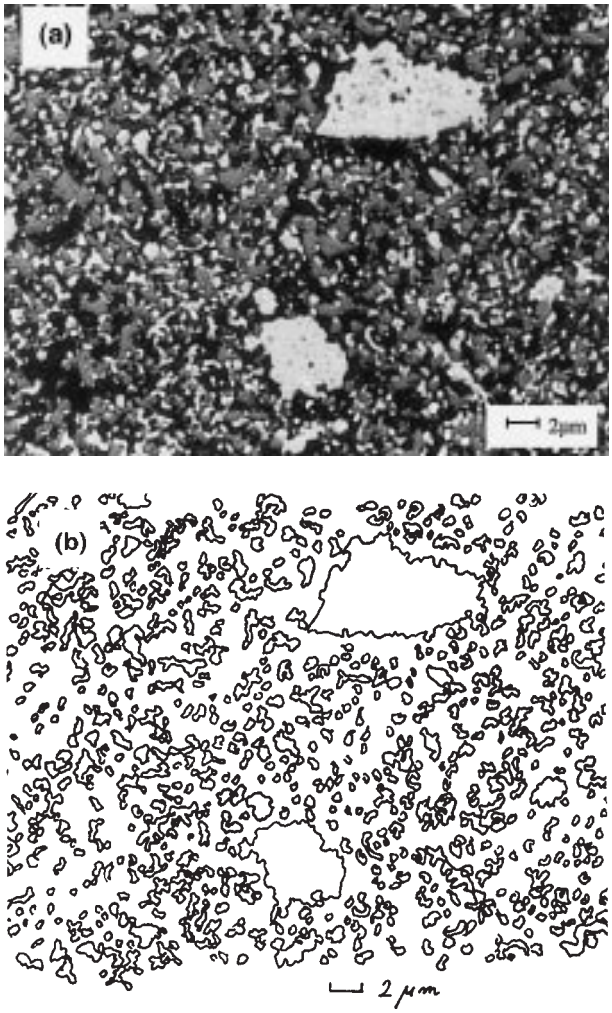

Fig. 8 (a) Micrograph of electrode Ab. Bright: electrolyte; grey: Ni agglomerates; black: pores. (b) Electrode Ab after nickel has been dissolved out.

partially in direct contact with the ceramic electrolytes. With the aid of the generally valid Equation 4, this nickel volume can then be converted into the envelope surface S_i. It is assumed that this surface should be directly proportional to the electrochemically active exchange surface if the rate of the electrochemical reaction is determined by the inhibition of the reaction kinetics. This establishes the first correlation between the number of interphases N_{t3} in a volume element and the contact surface S_i between the nickel and the YSZ electrolyte.

The volume integral functions determined in this way for all three electrodes studied are shown in Fig. 11. Using Equation 4, these functions can be converted into the corresponding surfaces S_i distribution curves shown in Fig. 12.

As can be seen from these Figures, the volume integrals of volume v_2 are in a pore radius region between $\log r \sim 2.6$ and 3.0, that is, between the pores with a diameter of 1 to 2 μm. The average spacing of single 'islands' in Fig. 8(b) of between 1–2 μm completely corresponds to the pore region of the volume integral from Fig. 11 determined by porosimetric measurements, which supports the above interpretation. The surface S_i enveloping the volume is formed by the pores at the lower boundary of this region. According to Fig. 12, the pore region of the surface S_i corresponds to the pores constituting the roughness of the single 'islands' and whose walls originate as the remains of the original nickel/electrolyte interphase in Fig. 8(a). These findings also support the above interpretation of the porosimetric curves. However, the estimated integral surface S_i is only a measure of the geometrical value of the envelope around the nickel particles and agglomerates in contact with the ceramic, where the actual nickel/ceramic interphase S_t only represents part of this total area. As a first approximation for this interphase we define the expression

$$S_t = knS_i \tag{5}$$

where n is the average number of contacts between all particles present in the electrode and k a proportionality factor for the fraction of the surface between the particles in contact per single contact. The following holds: $k \leqslant 1/n$. As a first approximation, it should be assumed that k is a constant. The product nS_i is then directly proportional to the active interface. It thus follows, according to Equation 3, that

$$\begin{aligned} knS_i &= S_t = \bar{S}_{t3}N_{t3} \\ j_0 &= \text{const.} \times knS_i \end{aligned} \tag{6}$$

This relation means that the porosimetrically determined metal/ceramic interphase nS_i can be regarded as a measure of the electrochemically active interphase. According to Karnaukhov's globular model of porous bodies [10], a theoretical dependence holds between the porosity ε and the number of particle contacts n, as illustrated in Table 3, so that the product number nS_i can be expressed as a function of the porosity ε.

This is shown by Table 4, which contains a summary of the electrochemical properties and porosity properties of the electrodes investigated. Since, according to Table 2, the number of optically determined three-phase boundaries, N_{t3}, in electrodes A and B is of equal size within experimental error, it is expected that the corresponding electrolyte interphase, nS_i, found by porosimetry will also be of the same size in the two electrode types within experimental error. As Table 4 shows, this was also confirmed. N_{t3} thus represents a measure of the electrochemical exchange current density j_0. After multiplication by k, the expression nS_i can therefore also serve as a measure of electrochemical activity. It is normally assumed that the internal surface of the electrode is the decisive criterion for evaluating electrochemical activity. Accordingly, the internal surfaces of the three measured electrodes would also have to be of equal size. Since, however, as can be seen from the values in Table 4, this is not the case, this assumption cannot be correct.

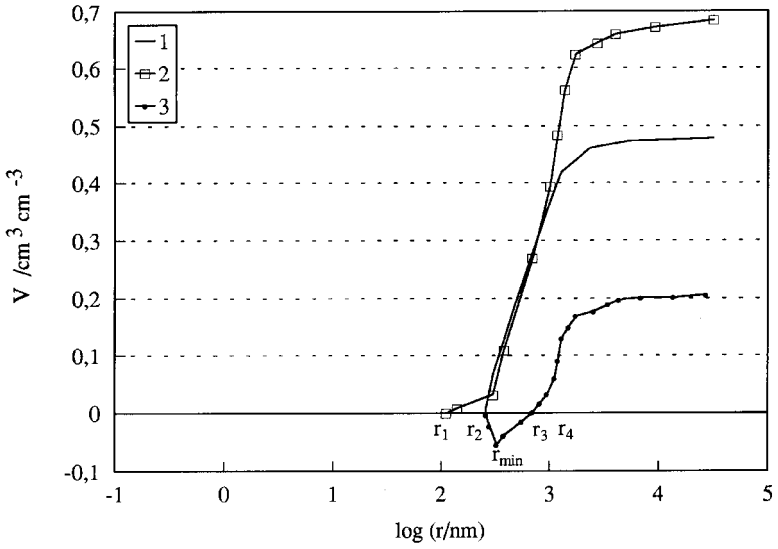

Electrode Aa

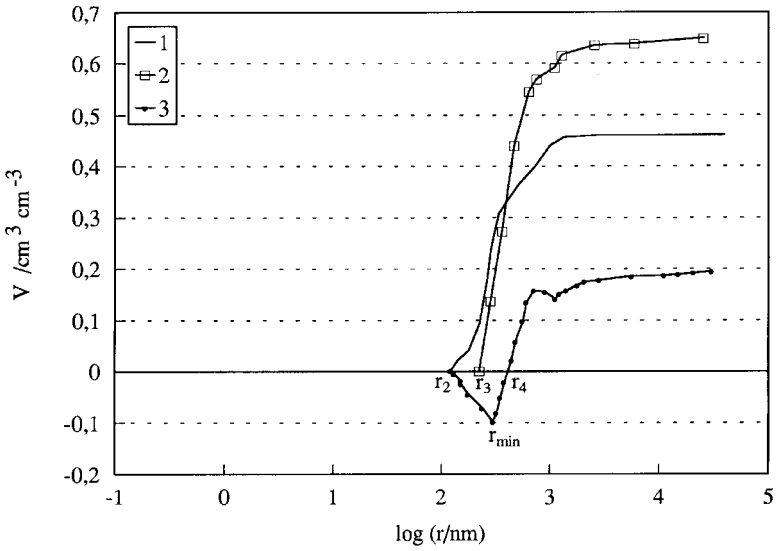

Electrode Ab

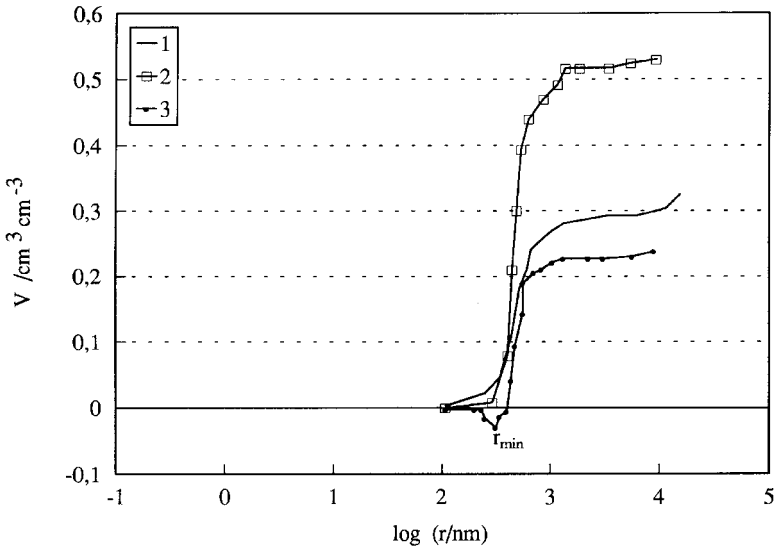

Electrode B

Fig. 9. Integral volume distribution as a function of pore radius. That is, (curve 1) original electrode, (curve 2) ceramic residual structure of the electrolyte and (curve 3) difference curve between 1 and 2.

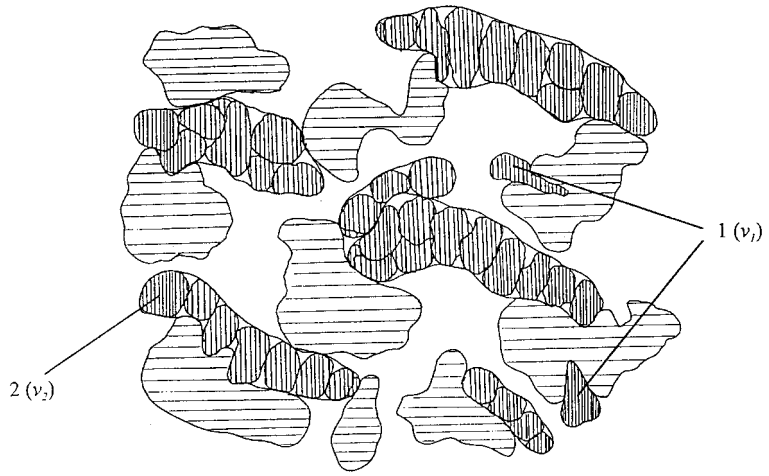

Fig. 10. Schematic representation of the cermet structure.

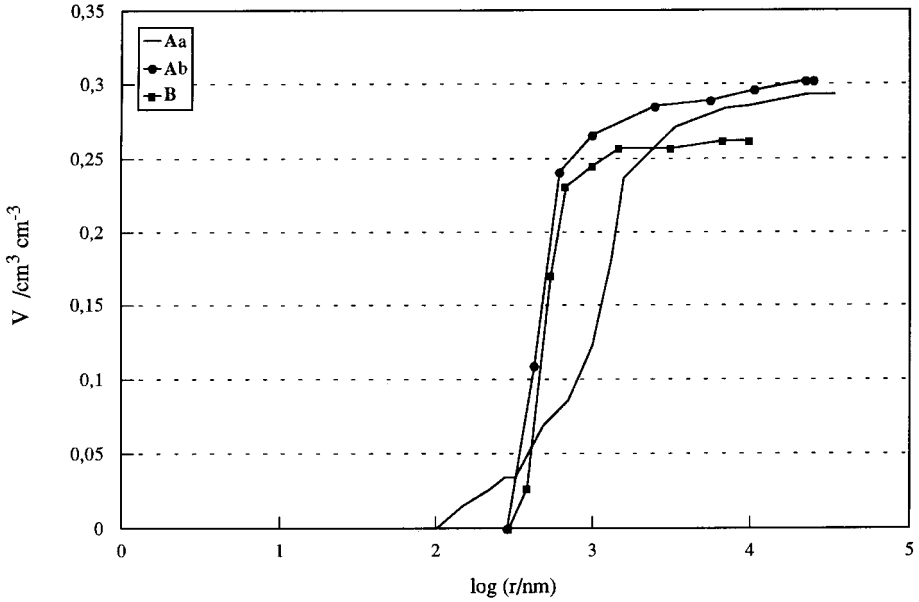

Fig. 11. Integral volume distribution of the Ni phase as a function of pore radius.

Table 3. Number of particle contacts n as a function of porosity ϑ

n	*12*	*8*	*6*	*4*	*3*	*2*
ε	0.2595	0.3198	0.4764	0.6599	0.8150	1.0 (extrapolated)

4. Conclusions

The results of the overall analysis for the SOFC cermet anodes show:

(i) There is a direct correlation between the number of optically visible 'electrolyte/nickel agglomerate/gas pore' three-phase boundaries in the unit volume of the electrode and the apparent electrochemical exchange current density representing a measure of the electrochemical kinetics.

(ii) The sum of the integrated volume of the nickel agglomerates and the single nickel particles in contact with the electrolyte gives the total amount of active nickel volume whose surface is, after consideration of the electrode porosity by

Table 4. Porosimetric properties of individual electrode types

Electrode	*Porosity ϑ*	*Internal surface* /m^2 cm^{-3}	*Residual porosity ϑ*	*volume, v_1* /%	*n*	S_i /m^2 cm^{-3}	nS_i /m^2 cm^{-3}
Aa	0.47	1.88	0.68	10	6.0	0.98	5.9
Ab	0.45	3.33	0.65	0	6.2	1.24	7.7
B	0.35	1.32	0.55	1	7.8	1.01	7.9

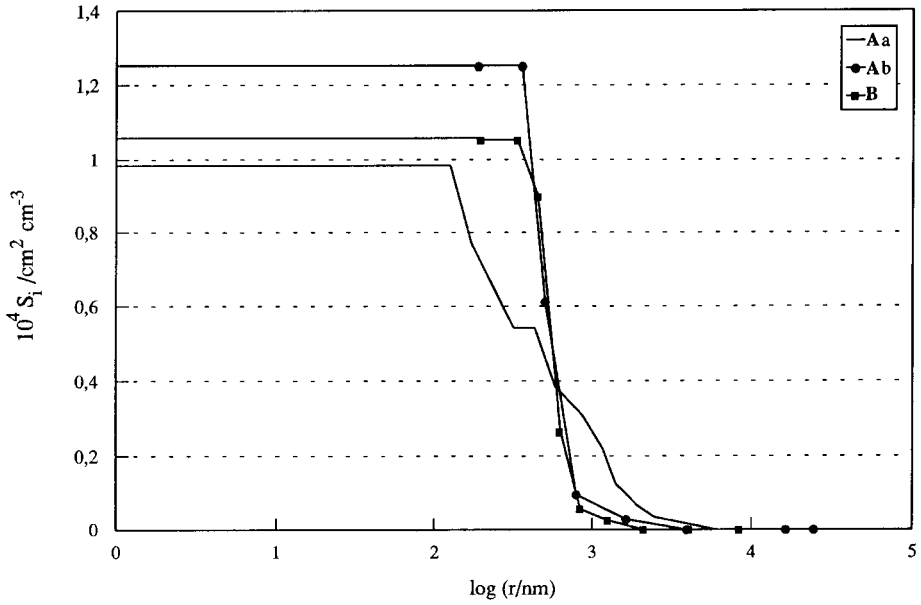

Fig. 12. Integral distribution of the outer surface of the Ni phase as a function of pore radius.

means of the number of contacts n, directly proportional to the amount of optically visible three-phase boundaries in the unit volume. It is therefore possible to predict the electrochemical kinetics of the SOFC cermet anode via the porosity measurements.

References

[1] N. Q. Minh, *J. Am. Ceram. Soc.* **76** (1993) 563.
[2] P. Holtappels, 'Die Elektrokatalyse an Nickel-Cermet Elektroden', Ph.D. Dissertation (University of Bonn, 1997).
[3] A. Winsel, *Z. Elektrochemie* **66** (1962) 287.
[4] J. Divisek, R. Jung and I. C. Vinke, *J. Appl. Electrochem.* **29** (1999) 165–170.
[5] A. Ruder, H. P. Buchkremer, H. Jansen, W. Mallener and D. Stöver, *Surf. Coat. Technol.* **53** (1992) 71.
[6] Y. Volfkovich and V. S. Bagotzky, *J. Power Sources* **48** (1994) 327.
[7] Y. Volfkovich and V. S. Bagotzky, *J. Power Sources* **48** (1994) 339.
[8] R. T. DeHoff, F. N. Rhines, 'Quantitative Microscopy' (McGraw-Hill, New York, 1968).
[9 Y. Volfkovich, E. I. Shkolnikov, V. S. Dubasova, and V. A. Ponomarev, *Elektrochimia* **19** (1983) 765.
[10] A. P. Karnaukhov, Structure, Classification and Simulation of Porous Materials, in: 'Pore Structure and Properties of Materials', Vol 1 (Prague, Academia, 1979), pp. A3–A33.